Bioconjugate Chemistry

Article

pubs.acs.org/bc

Graphene-Based "Hot Plate" for the Capture and Destruction of the Herpes Simplex Virus Type 1

Archana R. Deokar,[†,‡] Anjani P. Nagvenkar,[†,‡] Inna Kalt,[§] Lior Shani,[∥] Yosef Yeshurun,[∥] Aharon Gedanken,[*,†,‡] and Ronit Sarid[*,§]

[†]Department of Chemistry, Bar-Ilan University, Ramat Gan 5290002, Israel

[‡]Department of Materials Science and Engineering, National Cheng Kung University, Tainan 70101, Taiwan

[§]The Mina and Everard Goodman Faculty of Life Sciences, Bar-Ilan University, Ramat Gan 5290002, Israel

[∥]Department of Physics and Institute for Nanotechnology and Advanced Materials, Bar-Ilan University, Ramat Gan 5290002, Israel

S *Supporting Information*

ABSTRACT: The study of graphene-based antivirals is still at a nascent stage and the photothermal antiviral properties of graphene have yet to be studied. Here, we design and synthesize sulfonated magnetic nanoparticles functionalized with reduced graphene oxide (SMRGO) to capture and photothermally destroy herpes simplex virus type 1 (HSV-1). Graphene sheets were uniformly anchored with spherical magnetic nanoparticles (MNPs) of varying size between ∼5 and 25 nm. Fourier-transform infrared spectroscopy (FT-IR) confirmed the sulfonation and anchoring of MNPs on the graphene sheets. Upon irradiation of the composite with near-infrared light (NIR, 808 nm, 7 min), SMRGO (100 ppm) demonstrated superior (∼99.99%) photothermal antiviral activity. This was probably due to the capture efficiency, unique sheet-like structure, high surface area, and excellent photothermal properties of graphene. In addition, electrostatic interactions of MNPs with viral particles appear to play a vital role in the inhibition of viral infection. These results suggest that graphene composites may help to combat viral infections including, but not only, HSV-1.

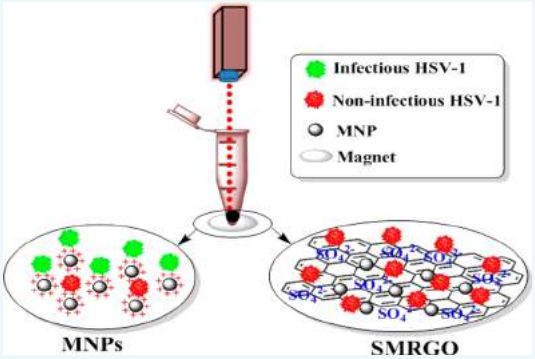

INTRODUCTION

Several worldwide human diseases are caused by viral infections, while emerging and re-emerging viruses represent major threats. For example, the largest outbreak of the Ebola virus infection in history occurred recently in 2014 in West Africa, while a recent spread of the Zika virus, accompanied by an unprecedented rise in birth defects, represents a current major health challenge.

Alike Ebola and Zika virus infections Herpes Simplex Virus type 1 (HSV-1) and -2 are also globally common.[1,2] The outcome of these infections includes a wide variety of clinical manifestations, ranging from asymptomatic infection to oral cold sores, genital ulceration, keratitis, and conjunctivitis. Complications, especially in neonates and immune suppressed patients, may lead to blindness and severe encephalitis. While vaccines may hold great promise as a prevention strategy, hurdles to the development of effective and safe vaccines persist, and no commercialized vaccines for HSV are presently available. The HSV infectious virions are 170−200 nm in diameter and consist of a large double-stranded DNA genome enclosed by icosahedral capsids that are surrounded by a lipid bilayer envelope containing 12 different virally encoded glycoproteins. Certain virion glycoproteins bind heparin sulfate (HS) moieties on the surface of the host cells, thereby promoting virion attachment and entry into susceptible cells. It is worth mentioning that interaction with host cell HS is the most common pathway for attachment by several other human and animal viruses as well.[3] HS is a ubiquitous negatively charged linear polymer composed of alternating moieties of hexuronic acid and glucosamine, sulfated at various positions.[4,5] In our group, efforts were taken to mimic HS on silver, gold NPs and graphene with mercaptoethanol sulfonate functionalization, thereby reducing the chance of HSV-1 infection through a competitive mechanism of host-cell attachment.[2,6,7]

Graphene, rising star of carbon-based materials, has been extensively studied because of its superior properties such as its large surface area (∼2700 m^2/gram), extreme thinness, and excellent thermal and electrical conductivity.[8−10] Graphene possesses excellent light-to-heat conversion ability owing to its superior thermal conductivity. Hence, it has been extensively explored under near-infrared (NIR) irradiation for photothermal (PTT) and photodynamic (PDT) treatment of cancer and bacterial inactivation.[11−13] Wu et al. designed a graphene-based rapid photothermal agent capable of inactivating both Gram-positive and Gram-negative bacterial strains within 10 min.[13] It has been observed that above 50 °C, bacterial enzymes

Received: January 19, 2017
Revised: February 7, 2017
Published: February 8, 2017

DOI: 10.1021/acs.bioconjchem.7b00030
Bioconjugate Chem. XXXX, XXX, XXX−XXX

Scheme 1. Stepwise Preparation of SMRGO[a]

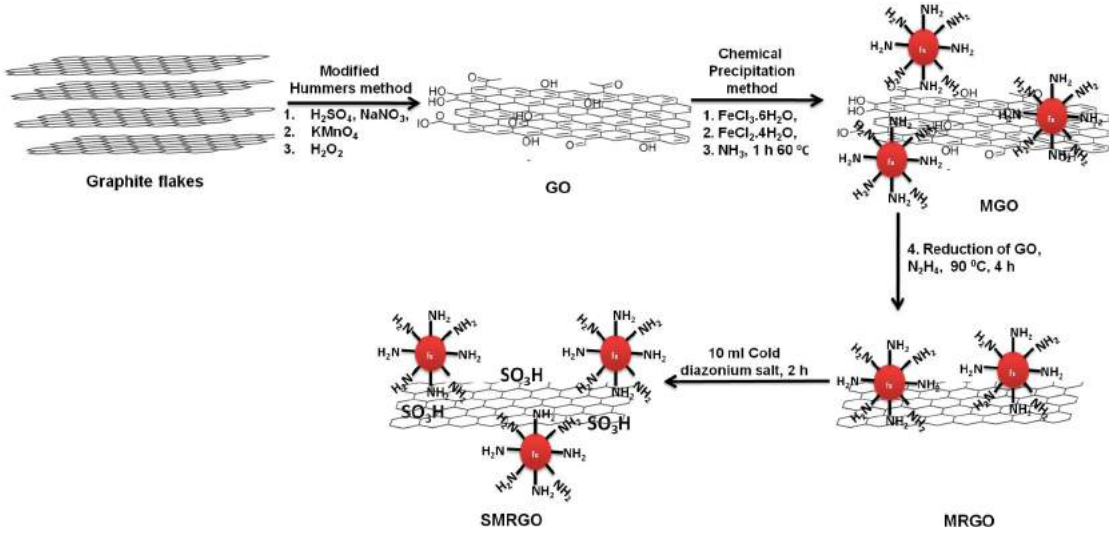

[a]First, graphite was oxidized to GO by a modification of Hummer's method. Next, the GO was functionalized with MNPs and reduced to MRGO. Last, the MRGO was sulfonated to yield SMRGO.

will denature and would inhibit necessary intracellular reactions, damage proteins and lipids in the cell membrane, and finally lead to bacterial death. PTT and PDT for treating viral infections are still at nascent stage. Recently, Ye et al. studied a single-layer reduced graphene oxide (RGO) as a potent antiviral agent and demonstrated that the sharp edges of the graphene oxide (GO), together with its negative charge, inactivate the porcine epidemic diarrhea virus.[14] A nanosized GO-based delivery system has also been explored for the simultaneous detection and breakdown of selected hepatitis C virus target genes.[15] Carbon nanohorns and buckminsterfullerene-based photothermal and photodynamic therapies have been employed for the destruction of bacteriophage, Semliki Forest, and vesicular stomatitis viruses, respectively.[16] Barras et al. also demonstrated that funtionalized carbon dots can effectively inhibit HSV-1.[17] Nevertheless, graphene-based photothermal antiviral therapy has not yet been studied. In this study, efforts have been made for the first time to design and synthesize an efficient graphene-based photothermal antiviral agent that captures and destroys viruses. We show that graphene functionalized with magnetic NPs and sulfonate groups can capture viruses that are then aggregated by an external magnet. By taking advantage of the superior photothermal properties of graphene, the captured viruses are inactivated with NIR irradiation and thus lose their ability to infect cells.

RESULTS AND DISCUSSION

The synthesis of sulfonated magnetic reduced graphene oxide (SMRGO) involves three steps, according to Scheme 1. GO (Scheme 1) was synthesized using a modification of Hummer's method, followed by simultaneous reduction and functionalization with magnetic nanoparticles (MNPs) using a chemical precipitation method to yield magnetic reduced graphene oxide (MRGO). Finally, the MRGO underwent sulfonation to mimic heparan sulfate moieties on cells. The magnetic properties of SMRGO enhanced the antiviral photothermal efficiency of graphene by concentrating the captured virions at one point using an external magnet.

Characterization. The morphology of SMRGO and MRGO was observed by transmission electron microscopy (TEM, Figure 1a and Figure 1b). Spherical MNPs with varying

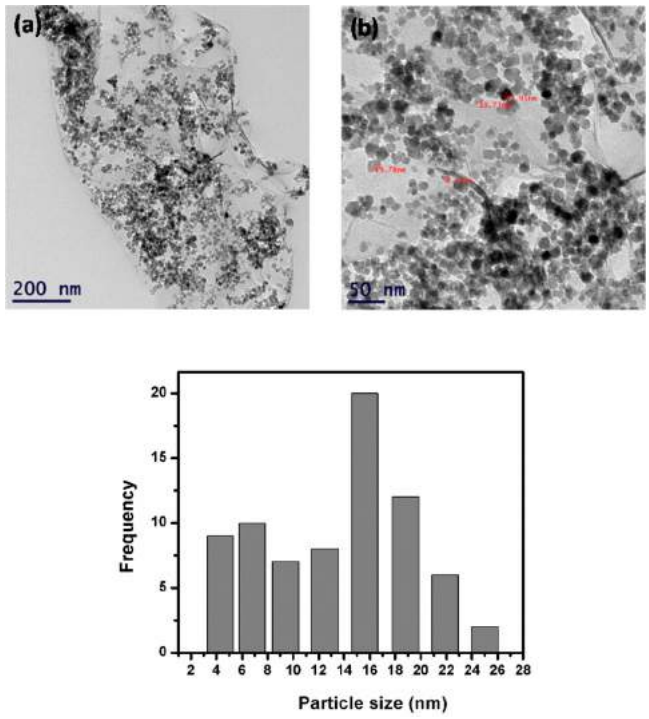

Figure 1. (a) TEM image of SMRGO, (b) a magnified view of image a, and (c) size distribution of MNPs anchored onto graphene sheets, determined by measuring a diameter of MNPs.

sizes of ~5−25 nm were uniformly anchored onto graphene sheets (Figure 1c). The reduction of GO to RGO is confirmed by Raman spectroscopy (Figure S2). The carbon-based materials show two main bands (D line around 1350 cm^{-1} and G line around 1580 cm^{-1}) in the Raman spectra. The intensity ratio of I_D/I_G for GO is 1.14 while for RGO it is 1.64

DOI: 10.1021/acs.bioconjchem.7b00030
Bioconjugate Chem. XXXX, XXX, XXX−XXX

which is much higher. The increased intensity confirms that GO is reduced by hydrazine to RGO.[18]

Fourier-transform infrared (FT-IR) spectroscopy (Figure 2) confirms the synthesis of the GO, MNPs, MRGO, and SMRGO. Figure 2a shows absorption bands for O−H stretching (a broad band at 2700−3700 cm^{-1} centered at about 3250 cm^{1}), aromatic and sp^2 C═C bonds (1680 cm^{-1}), the surface carboxylic group C═O−O (1720 cm^{-1}), epoxy C−O (1225 cm^{-1}), and alkoxy C−O (1050 cm^{-1}). All stretching frequencies confirm the successful oxidation of graphite to graphite oxide. MNPs which were anchored onto graphene sheets are surrounded by amine groups; hence primary amine N−H band at 3400 cm^{-1} and Fe−O bond at 575 cm^{-1} confirms the formation of MNPs (Figure 2b and Figure 2c) on graphene. Most of the oxygen-containing functional groups disappear in Figure 2c, confirming the successful reduction of GO to RGO. Figure 2d represents an additional stretching frequency at 1007 cm^{-1} that confirms the sulfonation and *p*-disubstituted phenyl group; this is in accordance with our previous study.[7] Thus, the FT-IR confirms the stepwise transition of GO to SMRGO.

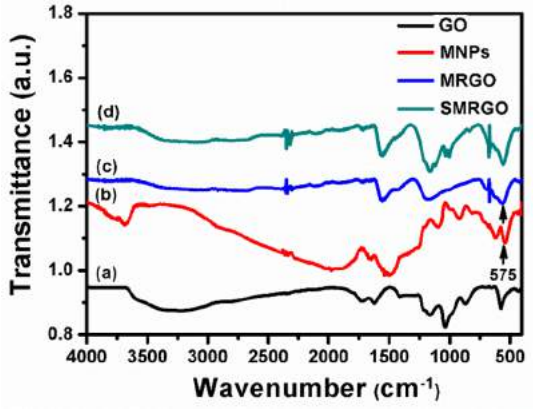

Figure 2. FT-IR spectrum of (a) GO, (b) MNPs, (c) MRGO, and (d) SMRGO.

The magnetic properties of MRGO and SMRGO were studied using a superconducting quantum interference device (SQUID) (MPMS-XL5, Quantum Design) at 300 K. Figure 3 depicts the measured magnetization vs the external magnetic field, demonstrating the superparamagnetic properties of MRGO and SMRGO, with a saturation value of $M_s \approx 28$ and $M_s \approx 21$ emu per gram of the measured material, respectively. No drastic change was observed in the saturation value of MRGO after its sulfonation. The X-ray diffraction (XRD) pattern of MNPs (Figure 4a) confirms the formation of Fe_3O_4 nanoparticles with peaks matching the JCPDS powder diffraction file no. 65-3107. The successful anchoring of MNPs on RGO is depicted in the XRD spectrum of MRGO (Figure 4b) with the peaks centered around $2\theta = 15°$ and 25° arising from the RGO (Figure S3). Sulfonation of MRGO did not affect the lattice structure of SMRGO indicated from the XRD pattern (Figure 4c)

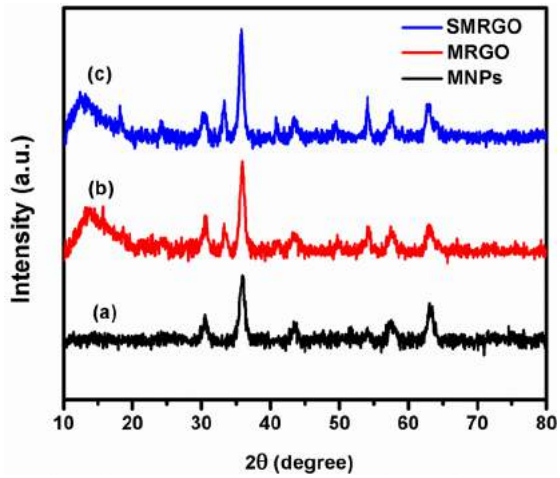

Figure 4. XRD pattern of (a) MNPs, (b) MRGO, and (c) SMRGO.

MNPs, MRGO, and SMRGO display optical density (OD) from the UV to NIR region (Figure 5 and Figure S4) with absorbance of 0.28, 1.12, and 1.23 at 808 nm, respectively. The photothermal efficiency of the MNPs, MRGO, and SMRGO was evaluated by irradiating their prepared solutions in phosphate buffer saline (PBS, pH = 7) with an NIR laser (808 nm, 1.6 W/cm^2, 10 min) and portrayed as a function of time.

The temperature evolution profile of the PBS (serving as a control), MNPs, MRGO, and SMRGO is represented in Figure 6. Two different concentrations, 100 and 1000 ppm, were employed to study the photothermal behavior of the MNPs, MRGO, and SMRGO. SMRGO demonstrates better photo-

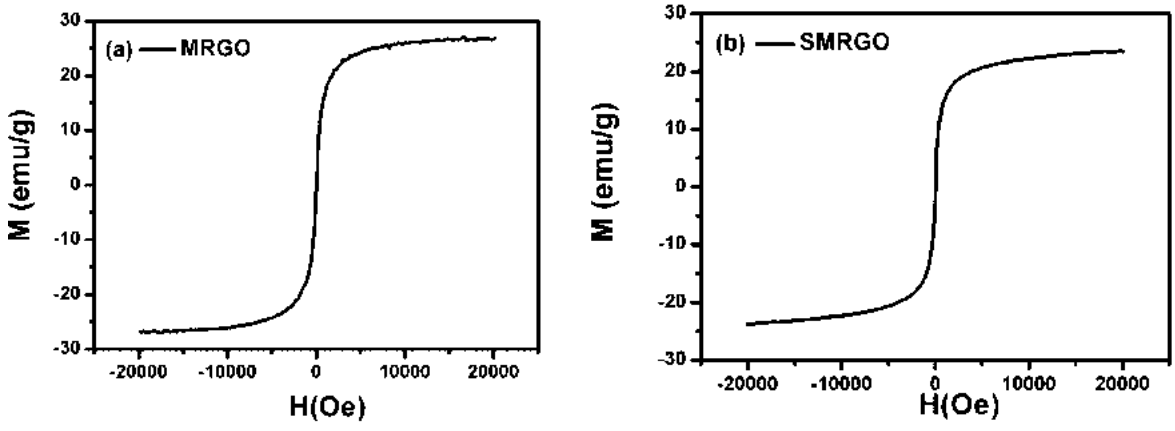

Figure 3. SQUID measurements for (a) MRGO and (b) SMRGO at 300 K.

DOI: 10.1021/acs.bioconjchem.7b00030
Bioconjugate Chem. XXXX, XXX, XXX−XXX

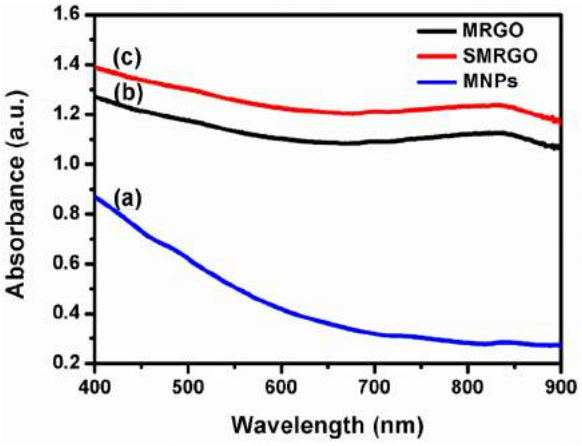

Figure 5. UV−vis−NIR spectra of (a) MNPs, (b) SMRGO, and (c) MRGO.

thermal efficiency for both 1000 (Figure 6a) and 100 ppm (Figure 6b) concentrations. Within 10 min, the temperature of both concentrations rose above 60 °C. The photothermal efficacy of the PBS is almost negligible compared to that of the MNPs/MRGO/SMRGO (Figure 6a and Figure 6b). Within 10 min, a temperature change from 26 to 34 °C in the PBS solution was recorded; the SMRGO underwent a drastic change in temperature from ∼26 to 61 °C at a concentration of 100 ppm (Figure 6a) and from ∼26 to 70 °C at a concentration of 1000 ppm. The temperature of the MRGO changed from ∼25 to 58/68 °C at concentrations of 100 and 1000 ppm, respectively. In spite of the sulfonation of the MRGO, the SMRGO demonstrated better photothermal efficiency, suggesting that fewer defects were introduced into the graphene. Thus, functionalization had little effect on the properties of GO. In this paper, we use the photothermal properties of graphene and the capture ability of the sulfonated moieties to effectively exclude and destroy HSV-1. Moreover, the MNPs play a vital role in aggregating the captured viral particles which, in turn, enhance the photothermal capability of the graphene. The ζ potential of the MNPs, MRGO, and SMRGO is depicted in Figure 7. The ζ-potential measurement depicts positive charge (+30.6 mV) on the MNPs due to the presence of positively charged ammonium groups, whereas the MRGO (−10.4 mV) and SMRGO (−16.7 mV) show negative charge due to incomplete reduction of the GO and sulfonation of the MRGO.

The stability of MNPs on MRGO and SMRGO is evaluated by conducting time dependent leaching studies in PBS buffer solution (Figure S5). The MRGO and SMRGO (100 ppm) were dispersed in PBS buffer solution and incubated for certain time intervals. The data represent the strong anchoring of the MNPs onto the surface of RGO with a little concentration of metal ions being leached out into the buffer solution indicated by ICP analysis. This affirms the fact that the MNPs interact via a chemical bond on the surface of RGO.

Cytotoxicity Assay. An XTT-based colorimetric assay was performed to verify the potential toxicity of the MNPs/MRGO/SMRGO in Vero African green monkey kidney epithelial cells used for HSV-1 infection in this study. Figure 8 demonstrates the cell viability upon treatment with 100/1000 ppm MNPs/MRGO/SMRGO. Both concentrations of the MNPs lack toxicity to cells, whereas a decrease in cell viability is observed at 1000 ppm of MRGO/SMRGO. This is probably due to either the hydrazine used during the synthesis of the graphene or the aggregation of the sheets during their incubation with cells. In contrast, comparatively lower concentration of MRGO/SMRGO has limited cell toxicity. Moreover, MRGO/SMRGO with lower concentration (100 ppm) also demonstrates better photothermal properties (above 55 °C); hence it was chosen for further photothermal antiviral study.

Virus Capture Efficiency of MNPs and SMRGO. The efficiency of the capture of infectious virions, as well as the destructive abilities of the MNPs/SMRGO, was studied using the plaque reduction assay. This assay provides a measurement of infectious virions that lyse cells and are capable of generating plaques. First, to evaluate the capture efficiency of the MNPs/SMRGO, we incubated 100 plaque-forming units (PFUs) of HSV-1 with 100 ppm of MNPs/SMRGO in absence of irradiation for 10 min (Scheme 2a). The captured virions along with the MNPs/SMRGO were then pulled down by an external magnet (Scheme 2b). Pellets of HSV-1 virions along with MNPs/SMRGO and suspensions containing floating unbound virions were assayed by plaque assay on 24-well plates (Scheme 2d,e).

The control includes HSV-1 virions that were treated similarly but in the absence of MNPs/SMRGO (control). Table 1 presents the results of a plaque assay obtained after incubation of HSV-1 with MNPs/SMRGO (Experimental Section). Interestingly, almost equal capture efficiency of infectious virions was evident with the MNPs (∼65.03%) and

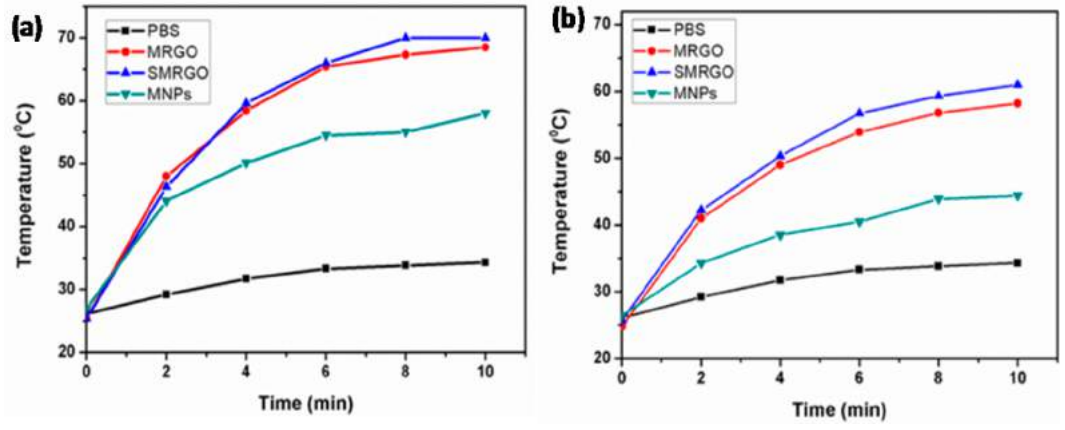

Figure 6. Temperature evolution profile at (a) 1000 ppm and (b) 100 ppm for PBS, MRGO, SMRGO, and MNPs as a function of time.

DOI: 10.1021/acs.bioconjchem.7b00030
Bioconjugate Chem. XXXX, XXX, XXX−XXX

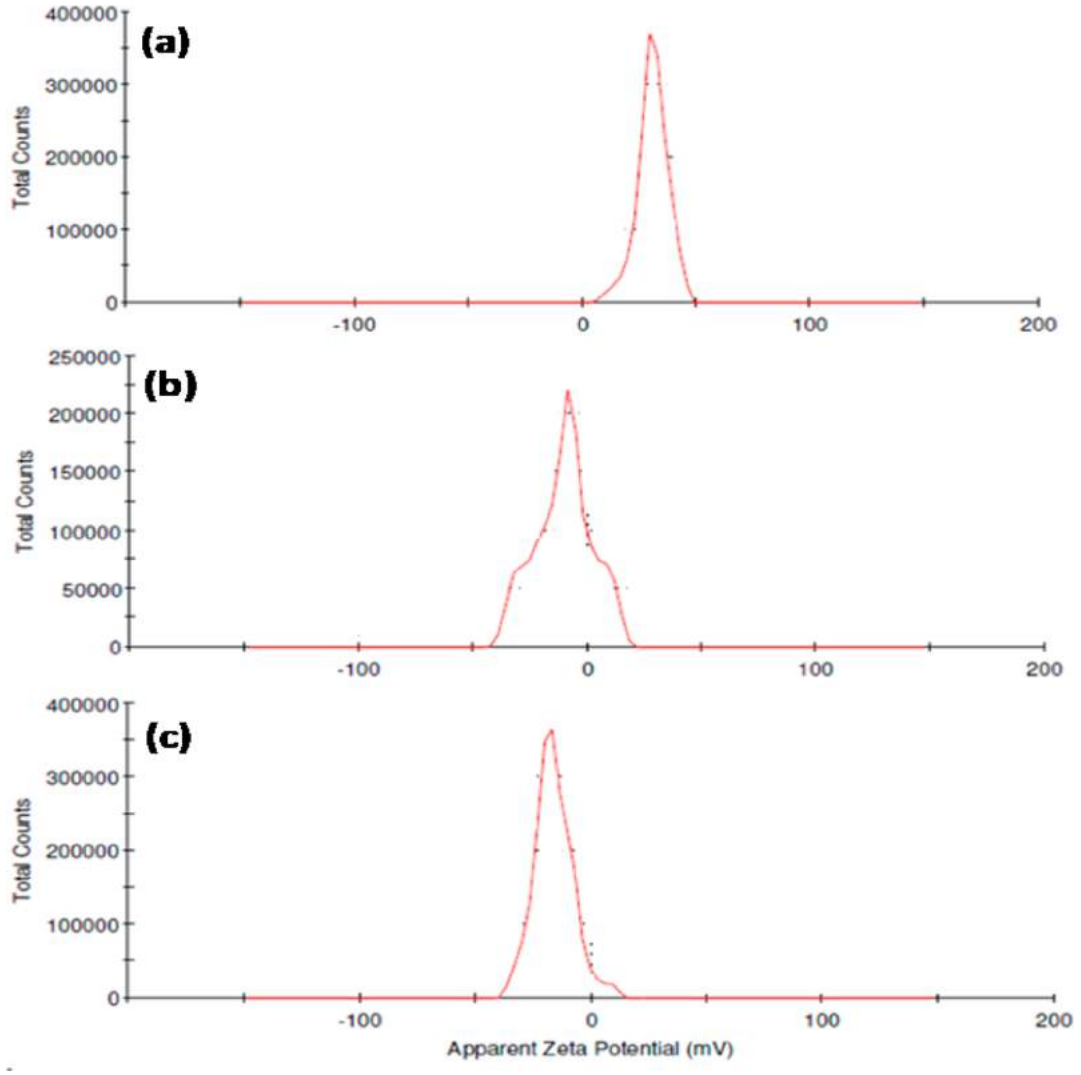

Figure 7. ζ potential for (a) MNPs, (b) MRGO, and (c) SMRGO.

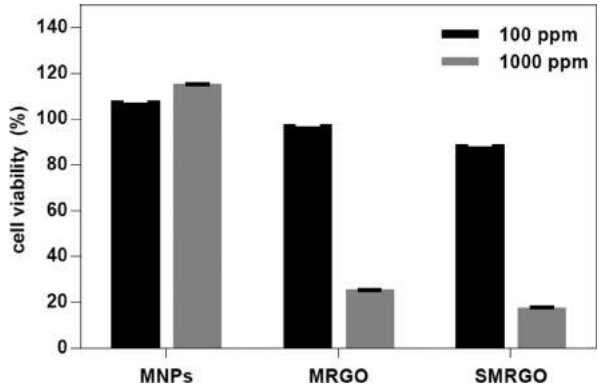

Figure 8. Cell cytotoxicity assay: Vero cell monolayers were grown in 96-well plates (2.5×10^4 cells/well) with 5% FCS in MEM Eagle medium. MNPs, MRGO, and SMRGO were added at the indicated ppm, and XTT measurements were performed 24 h later. The results are presented as the percentage of viable cells relative to the control untreated cells.

SMRGO (~65.62). Although charges for MNPs and SMRGO differ, both were competing equally to capture virions. It has been observed that growth medium masks NP's surface and affects its stability. In our previous study we have demonstrated experimentally that growth medium affects antiviral property of GO and RGO-SO_3.[7] Growth medium masks positively charged MNPs; hence it shows almost similar capture efficiency as of SMRGO. Mishra et al. demonstrate that partially negatively charged zinc oxide NPs tend to interact more effectively toward HSV-1/2 due to its ionic interactions with positively charged viral envelope of glycoproteins.[19]

Photothermal Antiviral Activity of MNPs and SMRGO. Photothermal antiviral activity was examined as shown in Scheme 2. The MNP/SMRGO-captured virions were immediately exposed to NIR irradiation (808 nm, 1.6 W/cm^2) for 7 min. The irradiated virions were then plated on cells in 24-well plates. Table 1 presents quantitative measurements of PFU before and after exposure to NIR light. As shown, NIR-irradiated virions were completely inactivated, and hence no further infection of host cells was observed (Table 1, Figure 9). SMRGO (100 ppm, Figure 6) has photothermal efficiency above 55 °C, while above 50 °C the HSV-1 virus starts to become inactive. Hence, after photothermal treatment with SMRGO, the virions were not able to infect host cells.[20,21] In contrast, MNPs do possess a good capture efficiency toward HSV-1, but due to their poor photothermal ability, they were unable to completely inactivate the HSV-1 virions (Table 1).

DOI: 10.1021/acs.bioconjchem.7b00030
Bioconjugate Chem. XXXX, XXX, XXX−XXX

Scheme 2. Photothermal Antiviral Assay for SMRGO/MNPs with or without NIR Irradiation (808 nm, 1.6 W/cm^2)

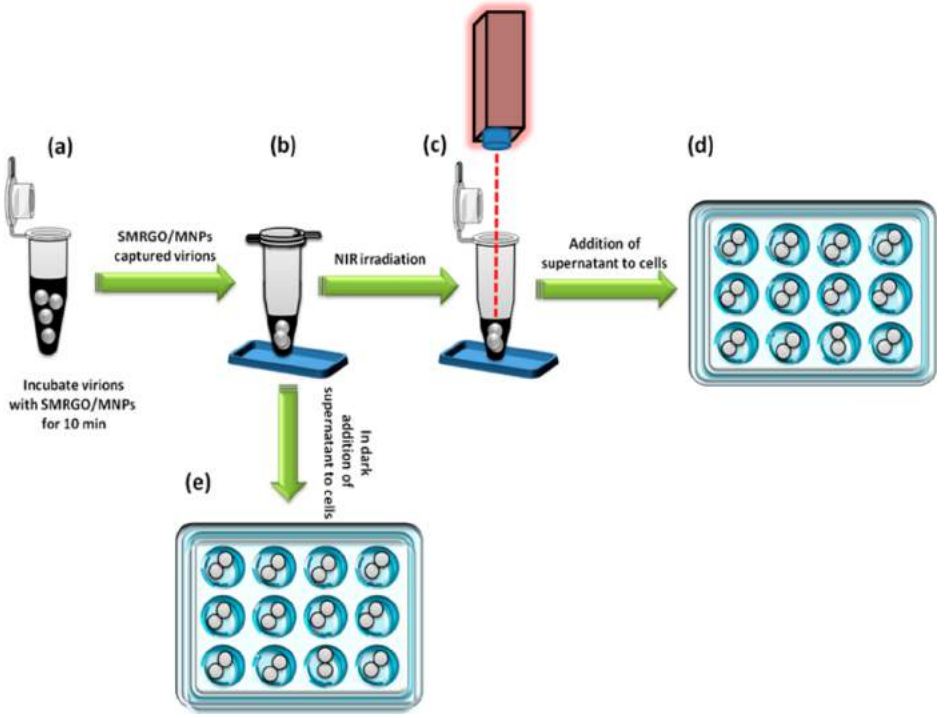

Table 1. Virion Capture Efficiency and Photothermal Antiviral Therapy for MNPs and SMRGO[a]

	without NIR light irradiation (PFU)			under NIR irradiation (PFU)		
material	control	expt	% infection [(exptl/control) ×100]	control	expt.	% infection [(exptl/control) ×100]
MNPs	169	135	79.88	117	35	29.91
	190	131	68.94	82	27	32.92
	201	93	46.26	70	0	0
			65.03 ± 17.14			**20.94 ± 18.20**
SMRGO	169	124	73.37	117	0	0
	190	160	84.21	82	0	0
	201	79	39.30	70	0	0
			65.62 ± 23.43			**0**

[a]Considering the total capture ability of the MNPs/MRGO pellet, capture efficiency was calculated based on the percentage of the cells infected by the virions in pellets after applying an external magnet with no light exposure.

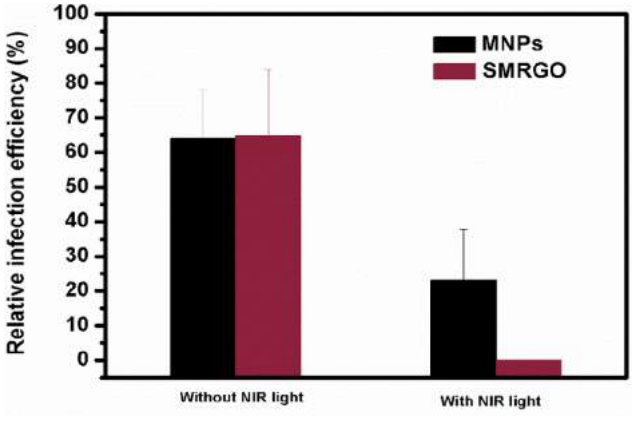

Figure 9. Relative percentage of cell infection before and after NIR irradiated photothermal treatment with MNPs and SMRGO.

The capture efficiency, unique sheetlike structure, high surface area, and better photothermal ability of graphene effectively eliminated the infectivity of the HSV-1 virions within 10 min. Song et al. demonstrated that negatively charged GO efficiently captures EV71 and H9N2; moreover they destroyed captured viruses by heating it to 56 °C for 30 min.[10] GO needs a high dose/power for photoablation due to suboptimal absorption of NIR light by GO in oxidized form.[22] Hence we choose RGO over GO; moreover magnetic properties of SMRGO help to aggregate captured viruses to one point which makes photothermal treatment more efficient (~99.9%) and rapid (within 10 min).

CONCLUSIONS

SMRGO was demonstrated to be an effective and rapid (~99.99%, 7 min) antiviral agent. Ease of functionalization of graphene with MNPs enables aggregation of captured viruses at a given point by using an external magnet, and hence it promotes effective photothermal treatment. MNPs were competing equally with SMRGO to capture virions. Graphene-based photothermal antiviral properties can allow the exclusion of infectious virions from contaminated sources. As

DOI: 10.1021/acs.bioconjchem.7b00030
Bioconjugate Chem. XXXX, XXX, XXX−XXX

interaction with host cell HS is the most common pathway for attachment by several other human and animal viruses, this study potentially can be employed not only against HSV-1 but also for several other viruses.

EXPERIMENTAL SECTION

Synthesis of GO. Graphite flakes were oxidized to GO by a modification of Hummer's method (Purity 99%, Alfa Aesar, USA)).[23] A conical flask equipped with a magnetic stirring bar was charged with H_2SO_4 (69 mL) and cooled at 0−5 °C. Graphite flakes (1.5 g) were then added slowly with vigorous stirring, followed by slowly adding $KMnO_4$ (4.5 g) and $NaNO_3$ (1.5 g) for 15 min. The temperature of the reaction mixture was maintained at 0−5 °C during the addition process. The mixture was allowed to warm to room temperature (RT) and stirred for 1 h. The RT mixture was charged with double-distilled water (DDW) (120 mL) and stirred for 30 min while the temperature was raised to 90 °C. The mixture was poured into DDW (300 mL), followed by the slow addition of 10 mL of H_2O_2. The solution color subsequently changed from dark-brown to yellow. The remaining solution was filtered. The residual material was redispersed in DDW and washed until the filtrate pH became neutral. The resultant GO material was dried overnight in vacuum, at RT.

Synthesis of MRGO. The GO sheets were further functionalized with MNPs by a chemical precipitation method.[24] GO (0.35 g) was exfoliated in DDW by sonication. Iron(III) chloride hexahydrate ($FeCl_3{\cdot}6H_2O$, 0.35 g) and iron(II) chloride tetrahydrate ($FeCl_2{\cdot}4H_2O$, 0.2 g) (purity 99%, Merck, Germany) with a ratio of 2:1, used as Fe sources, were dissolved in DDW (50 mL) and added slowly to the GO suspension. The ammonia solution (0.5 mL) was quickly added and stirred for 1 h at 60 °C to yield the precipitating MNPs. An amount of 500 μL of hydrazine was added for 4 h at 90 °C to reduce the GO to RGO. The MRGO product was washed three times with DDW and dried in vacuum overnight.

Synthesis of SMRGO. The synthesis of sulfonated MRGO (SMRGO) was carried out as in the previous study.[6] 0.075 g of MRGO was dispersed in 75 mL of DDW by bath sonication for 30 min. 10 ml of cold diazonium solution (0.046 sulfanilic acid, 0.018 g of sodium nitrite in 10 mL DDW, and 0.5 mL of 1 M HCl solution) were allowed to interact with MRGO under constant stirring at 5 °C for 2 h. The resultant sulfonated MRGO was washed thoroughly with DDW and dried under vacuum.

Characterization of SMRGO. The chemical composition and morphology of the resultant SMRGO was studied by TEM, FT-IR, UV−vis-NIR spectroscopy, and a superconducting quantum interference device (SQUID). The UV−vis-NIR spectra of the MNPs, MRGO and SMRGO were recorded on a CARY bio-100 spectrophotometer. The FT-IR data was recorded on an Avarter model FT-IR spectrometer. The magnetic properties of the material were investigated using an MPMS-XL5 Quantum Design SQUID.

Cells and Viruses. Plaque reduction assay was performed by using Vero African green monkey kidney epithelial cells grown in a 24-well plate in minimum essential media (MEM) Eagle's medium (Biological Industries, Israel), supplemented with 10% heat-activated fetal calf serum (FCS) (Biological Industries), L-glutamine, and penicillin−streptomycin−amphotericin (PSA) (Biological Industries). The cells were maintained at 37 °C under 5% CO_2. The virus used was a wild-type HSV-1 McIntyre strain.

HSV-1 in Vitro Photothermal Assay. Viral infection was evaluated by a plaque assay on Vero cells. Cells were plated in 24-well plates (4.5×10^5 cells/well). Viral suspensions (1000 PFU) were incubated for 7 min with MNPs/MRGO/SMRGO (100/1000 ppm) prior to their introduction into cells. The MNPs/MRGO/SMRGO-treated viral suspensions were pulled down with an external magnet (Scheme 2) and immediately subjected to NIR light irradiation (808 nm, 1.6 W/cm^2). The NIR-irradiated SMRGO viral suspensions suspended in a medium were added to the cells at 37 °C. The control included an untreated viral suspension, viruses that were only irradiated, and viruses that were incubated with particles but did not undergo irradiation. After 48 h of incubation, the cell monolayers were stained with Giemsa and the plaques were counted.

Cytotoxicity Assay. A 2,3-bis(2-methoxy-4-nitro-5-sulfophenyl)-2*H*-tetrazolium-5-carboxanilide (XTT) based colorimetric assay was performed in order to confirm the lack of cell toxicity in the MNPs/MRGO/SMRGO. The assay was carried out according to the manufacturer's protocol (Biological Industries), and absorbance was measured using a TECAN Spectrafluor Plus (NEOTEC Scientific Instrumentation Ltd.) spectrophotometer at a 405 nm wavelength. Vero-cell monolayers were grown in 96-well plates (2.5×10^4 cells/well) with 5% FCS in MEM Eagle's medium at 37 °C under 5% CO_2. MNPs/MRGO/SMRGO was added into each well at different concentrations (100−1000 ppm). The control consisted of Vero-cell monolayers without MNPs/MRGO/SMRGO. The cytotoxicity was examined using an XTT cell viability assay based on OD measurements, which are proportional to the number of living cells in the sample.

ASSOCIATED CONTENT

Supporting Information

The Supporting Information is available free of charge on the ACS Publications website at DOI: 10.1021/acs.bioconjchem.7b00030.

TEM images of GO and SMRGO, XRD and Raman spectra of GO and RGO, UV−vis spectra of MNPs, MRGO, and SMRGO, plot of time dependent leaching studies of MRGO and SMRGO and tables indicating the virion capture efficiency of MRGO, photothermal antiviral therapy data of MRGO, and ζ potential values of MNPs, MRGO, and SMRGO (PDF)

AUTHOR INFORMATION

Corresponding Authors

*E-mail: Aharon.Gedanken@biu.ac.il.

*E-mail: saridr@mail.biu.ac.il

ORCID

Aharon Gedanken: 0000-0002-1243-2957

Author Contributions

⊥A.R.D. and A.P.N. equally contributed to this work.

Notes

The authors declare no competing financial interest.

REFERENCES

(1) Adhikary, R. R., More, P., and Banerjee, R. (2015) Smart Nanoparticles as Targeting Platforms for HIV Infections. *Nanoscale* 7, 7520−7534.

(2) Baram-Pinto, D., Shukla, S., Perkas, N., Gedanken, A., and Sarid, R. (2009) Inhibition of Herpes Simplex Virus Type 1 Infection by

DOI: 10.1021/acs.bioconjchem.7b00030
Bioconjugate Chem. XXXX, XXX, XXX−XXX

Silver Nanoparticles Capped with Mercaptoethane Sulfonate. *Bioconjugate Chem. 20*, 1497−1502.
(3) Mardberg, K., Trybala, E., Glorioso, J. C., and Bergstrom, T. (2001) Mutational analysis of the major heparan sulfate-binding domain of herpes simplex virus type 1 glycoprotein C. *J. Gen. Virol. 82*, 1941−1950.
(4) Reske, A., Pollara, G., Krummenacher, C., Chain, B. M., and Katz, D. (2007) Understanding HSV-1 Entry Glycoproteins. *Rev. Med. Virol. 17*, 205−215.
(5) Szunerits, S., Barras, A., Khanal, M., Pagneux, Q., and Boukherroub, R. (2015) Nanostructures for the Inhibition of Viral Infections. *Molecules 20*, 14051−14081.
(6) Baram-Pinto, D., Shukla, S., Gedanken, A., and Sarid, R. (2010) Inhibition of HSV-1 Attachment, Entry, and Cell-to-Cell Spread by Functionalized Multivalent Gold Nanoparticles. *Small 6*, 1044−1050.
(7) Sametband, M., Kalt, I., Gedanken, A., and Sarid, R. (2014) Herpes Simplex Virus Type-1 Attachment Inhibition by Functionalized Graphene Oxide. *ACS Appl. Mater. Interfaces 6*, 1228−1235.
(8) Geim, A. K., and Novoselov, K. S. (2007) The Rise of Graphene. *Nat. Mater. 6*, 183−191.
(9) Chen, J., Peng, H., Wang, X., Shao, F., Yuan, Z., and Han, H. (2014) Graphene oxide exhibits broad-spectrum antimicrobial activity against bacterial phytopathogens and fungal conidia by intertwining and membrane perturbation. *Nanoscale 6*, 1879−1889.
(10) Song, Z., Wang, X., Zhu, G., Nian, Q., Zhou, H., Yang, D., Qin, C., and Tang, R. (2015) Virus Capture & Destruction by Label-Free Graphene Oxide for Detection & Disinfection Applications. *Small 11*, 1171−1176.
(11) Yang, K., Zhang, S., Zhang, G., Sun, X., Lee, S. T., and Liu, Z. (2010) Graphene in Mice: Ultrahigh in Vivo Tumor Uptake and Efficient Photothermal Therapy. *Nano Lett. 10*, 3318−3323.
(12) Ge, J., Lan, M., Zhou, B., Liu, W., Guo, L., Wang, H., Jia, Q., Niu, G., Huang, X., Zhou, H., et al. (2014) A Graphene Quantum Dot Photodynamic Therapy Agent with High Singlet Oxygen Generation. *Nat. Commun. 5*, 4596−4603.
(13) Wu, M.-C., Deokar, A. R., Liao, J.-H., Shih, P.-Y., and Ling, Y.-C. (2013) Graphene-Based Photothermal Agent for Rapid and Effective Killing of Bacteria. *ACS Nano 7*, 1281−1290.
(14) Ye, S., Shao, K., Li, Z., Guo, N., Zuo, Y., Li, Q., Lu, Z., Chen, L., He, Q., and Han, H. (2015) Antiviral Activity of Graphene Oxide: How Sharp Edged Structure and Charge Matter. *ACS Appl. Mater. Interfaces 7*, 21571−21579.
(15) Kim, S., Ryoo, S.-R., Na, H.-K., Kim, Y.-K., Choi, B.-S., Lee, Y., Kim, D.-E., and Min, D.-H. (2013) Deoxyribozyme-Loaded Nano-Graphene Oxide for Simultaneous Sensing and Silencing of the Hepatitis C Virus Gene in Liver Cells. *Chem. Commun. (Cambridge, U. K.) 49*, 8241−8243.
(16) Käsermann, F., and Kempf, C. (1997) Photodynamic inactivation of enveloped viruses by buckminsterfullerene. *Antiviral Res. 34*, 65−70.
(17) Barras, A., Pagneux, Q., Sane, F., Wang, Q., Boukherroub, R., Hober, D., and Szunerits, S. (2016) High Efficiency of Functional Carbon Nanodots as Entry Inhibitors of Herpes Simplex Virus Type 1. *ACS Appl. Mater. Interfaces 8*, 9004−9013.
(18) Yan, J., Fan, Z., Wei, T., Qian, W., Zhang, M., and Wei, F. (2010) Fast and Reversible Surface Redox Reaction of Graphene-MnO_2 Composites as Supercapacitor Electrodes. *Carbon 48*, 3825−3833.
(19) Mishra, Y. K., Adelung, R., Rohl, C., Shukla, D., Spors, F., and Tiwari, V. (2011) Virostatic potential of micro-nano filopodia-like ZnO structures against herpes simplex virus-1. *Antiviral Res. 92*, 305−312.
(20) Lelie, P. N., Reesink, H. W., and Lucas, C. J. (1987) Inactivation of 12 viruses by heating steps applied during manufacture of a hepatitis B vaccine. *J. Med. Virol. 23*, 297−301.
(21) Kaplan, C. (1958) The Heat Inactivation of Vaccinia Virus. *J. Gen. Microbiol. 18*, 58−63.
(22) Robinson, J.-T., Tabakman, S.-M., Liang, Y., Wang, H., Casalongue, H.-S., Vinh, D., and Dai, H. (2011) Ultrasmall Reduced Graphene Oxide with High Near-Infrared Absorbance for Photothermal Therapy. *J. Am. Chem. Soc. 133*, 6825−6831.
(23) Wang, S., Tang, L. A. L., Bao, Q. L., Lin, M., Deng, S. Z., Goh, B. M., and Loh, K. P. (2009) Room-Temperature Synthesis of Soluble Carbon Nanotubes by the Sonication of Graphene Oxide Nanosheets. *J. Am. Chem. Soc. 131*, 16832−16837.
(24) Lee, P.-L., Sun, Y.-C., and Ling, Y.-C. (2009) Magnetic nano-adsorbent integrated with lab-on-valve system for trace analysis of multiple heavy metals. *J. Anal. At. Spectrom. 24*, 320−327.

DOI: 10.1021/acs.bioconjchem.7b00030
Bioconjugate Chem. XXXX, XXX, XXX−XXX